

Analysis of the influence of current frequency on the thermal field of the insulated busbar

J. GOŁĘBIEWSKI and M. ZARĘBA *

Faculty of Electrical Engineering, Białystok University of Technology, 45D Wiejska St., 15-351 Białystok, Poland

Abstract. The paper analysed the influence of current frequency on the thermal field of the insulated busbar. Its physical model consist of two hollow cylinders and a solid cylinder with different material properties. In turn, the mathematical model is a system of heat conduction equations with the appropriate set of the boundary, initial and continuity conditions. The problem was solved using the modified Green's method. As a result, the following characteristics and parameters of the busbar were determined as a functions of frequency: heating curves, local time constants, steady-state current ratings, and stationary temperature profiles. The results were positively verified by finite element method.

Key words: frequency analysis, analytical methods, temperature field, insulated busbar.

1. Introduction

It is essential to analyse the thermal field generated by current in electric cables and busbars. The insulation temperature limits both the steady-state current rating [1, 2] and the short-time fault current. Exceeding these parameters may destroy the system; it always accelerates the aging of the insulating materials and reduces their reliability. In the case of alternating current, the thermal field distribution is also strongly influenced by the skin effect [3, 4]. It is connected with the displacement of current in the external direction that causes an uneven distribution of current density in the conductor. As a result, as the frequency increases, busbar resistance and thus the amount of heat released increase. Therefore, it is crucial to analyse the impact of current frequency on the thermal field in conductive systems.

Researchers have devoted numerous publications to the analysis of the frequency impact on electrical phenomena (e.g., on skin effect [5–8], dispersion [9, 10] or filtration of signals [11, 12]). However, publications that deal with the influence of frequency on the thermal field are relatively rare. Papers [13–15] are certain exceptions. In [13, 14], the authors developed a coupled electro-thermal model of an overhead power line taking into account the skin effect (and thus the influence of frequency). In [13, 14] the corresponding equations were solved numerically using the finite difference method. In [13], a two-layer (bimetallic) cylindrical configuration was investigated, while in [14] a single-layer (monometallic) structure was analysed. On the other hand, in [15], the thermal field in the bare conductor was calculated also considering the influence of frequency through skin effect. The analytical method of separation of variables [16, 17] was used in paper [15].

The subject of this paper is, however, a cylindrical three-region structure (a busbar insulated by means of a heat-shrinkable tube with an adhesive layer). Such systems are used, among others, in electrical substations and switchgear. In order to solve the appropriate boundary-initial problem, an analytical approach was also used, but based on Green's function [18, 19]. Some advantages of analytical methods, whose results are presented in the form of formulas, are worth mentioning here. They facilitate the discussion on the impact of the particular parameters and the physical interpretation of the obtained results. What is more, analytical solutions enable one to verify numerical calculations, estimate field at selected points and find the scaling laws.

The purpose of this paper is to determine the operational characteristics and parameters of the busbar. As frequency functions, the following is considered: steady-state current ratings, heating curves, local time constants, and stationary temperature profiles. The first of these parameters is essential for the thermal safety of the adhesive layer and insulation. Two further characteristics are crucial in the analysis of transient states (e.g., when switching the busbar on and off, changing the load, with discontinuous operation, etc.). In turn, stationary temperature profiles are used to assess the correctness of sustained operation.

2. The physical and mathematical model of the system

Fig. 1 shows the cross-section of the studied system. The internal area of the model is a solid copper busbar (index 1). Isolation is a heat-shrinkable tube made from a cross-linked polymer (index 3). It is extruded together with the inner adhesive layer (technical adhesives or cover materials – index 2). In practice, this structure protects the system against moisture and corrosive gases, while providing electrical insulation and mechanical protection. The above-described system is much longer than its

*e-mail: m.zareba@pb.edu.pl

Manuscript submitted 2019-03-29, revised 2019-05-31, initially accepted for publication 2019-06-25, published in February 2020

external diameter. Also, the insulated busbar is characterized by axial symmetry. Therefore, the thermal field is only a function of the radial coordinate and time. In addition, the material parameters of the system were averaged within the scope of the expected temperature change. The busbar is in constant temperature air T_a and is shielded from direct solar radiation and wind (in-door conditions). The flow of alternating current heats the system from the moment $t = 0$.

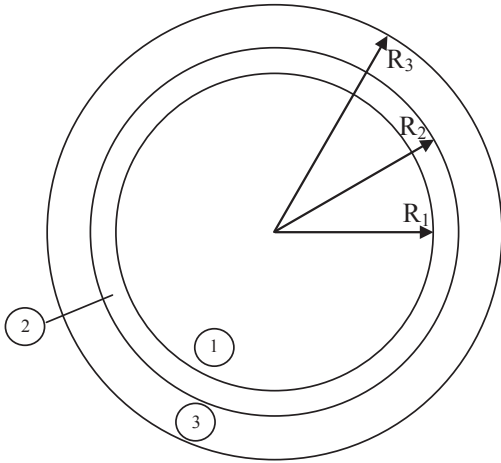


Fig. 1. Cross-section of an insulated busbar.

The boundary-initial problem of the model is presented in relation to the increments $v_i(r, t)$ related to ambient temperature T_a

$$v_i(r, t) = T_i(r, t) - T_a, \quad (1)$$

where: $i = 1$ (for copper), $i = 2$ (for adhesive layer), $i = 3$ (for insulation), $T_i(r, t)$ is the space-time field distribution, t denotes the time, r represents the radial coordinate.

The increment (1), with the aforementioned simplifying assumptions, is described by the following equation of heat conductivity [16, 20]

$$\frac{\partial^2 v_i(r, t)}{\partial r^2} + \frac{1}{r} \frac{\partial v_i(r, t)}{\partial r} - \frac{1}{\chi_i} \frac{\partial v_i(r, t)}{\partial t} = -\frac{g_i(r, f)}{\lambda_i} \quad (2)$$

$$\text{for } R_{i-1} \leq r \leq R_i, \quad t > 0, \quad i = 1, 2, 3,$$

where: $R_0 = 0$ and $\chi_i = \lambda_i / (c_i \delta_i)$ is diffusivity of the i -th region, λ_i , c_i , δ_i are thermal conductivity, specific heat and density of the i -th region, respectively, R_1 , R_2 , R_3 are consecutive radii of the system regions (Fig. 1). The power volume density in copper $g_1(r, f)$ was determined separately for alternating current and direct current. In the case of alternating current, dependence [4] was used

$$g_1(r, f) = \rho \cdot \left| \frac{mI}{2\pi R_1} \frac{I_0(mr)}{I_1(mR_1)} \right|^2, \quad (3a)$$

where $m = \sqrt{j2\pi f \mu_o / \rho}$, ρ is the average resistivity of a conductor, μ_o is the magnetic permeability of a vacuum, I is the rms value of alternating current, f is frequency, $j = \sqrt{-1}$ is an imaginary unit, $I_p(\dots)$ are modified Bessel functions of the

order p ($p = 0$ or $p = 1$). In the case of direct current, there is no skin effect, and the power volume density does not depend on r

$$g_{DC} = g_1(r, f = 0) = \frac{\rho I^2}{\pi^2 R_1^4} = \text{const}, \quad (3b)$$

where $I = I_{DC}$.

No heat sources are present in the insulation and the adhesive layer ($g_2(r, f) = g_3(r, f) = 0$). It was assumed that before turning on the power supply, the system was at ambient temperature T_a . The following initial conditions result from the definition of increment (1)

$$v_i(r, t = 0) = 0, \quad \text{for } R_{i-1} \leq r \leq R_i \quad \text{and } i = 1, 2, 3. \quad (4)$$

The external surface of the system (for $r = R_3$) gives up the heat by convection and radiation. The mentioned transfer is described by Hankel's boundary condition [20]

$$\left. \frac{\partial v_3(r, t)}{\partial r} \right|_{r=R_3} = -\frac{\alpha}{\lambda_3} v_3(r = R_3, t) \quad \text{for } t > 0, \quad (5)$$

where α is the total heat transfer coefficient (the sum of convection and radiation coefficients).

The individual layers of the insulated busbar adhere tightly to each other. Therefore, the conditions for continuity of temperature increase and heat flux are met at the boundaries of regions

$$v_i(R_i, t) = v_{i+1}(R_i, t) \quad \text{for } i = 1, 2 \quad \text{and } t > 0, \quad (6a)$$

$$\lambda_i \left. \frac{\partial v_i(r, t)}{\partial r} \right|_{r=R_i} = \lambda_{i+1} \left. \frac{\partial v_{i+1}(r, t)}{\partial r} \right|_{r=R_i} \quad (6b)$$

$$\text{for } i = 1, 2 \quad \text{and } t > 0.$$

Equations (2)–(6) formulate the boundary-initial problem of the model's transient field.

3. Green's functions

The boundary-initial problem (2)–(6) was solved by the Green's function $G_i = G_i(r, t, \xi, \eta)$ method [18, 20, 21]. In the three-region system analysed, G_i functions were defined [20, 21] as follows

$$\frac{\partial^2 G_i}{\partial r^2} + \frac{1}{r} \frac{\partial G_i}{\partial r} - \frac{1}{\chi_i} \frac{\partial G_i}{\partial t} = -\varphi_i \quad (7)$$

for $R_{i-1} \leq r \leq R_i$, $t \geq \eta$, $R_0 = 0$, $i = 1, 2, 3$, where

$$\varphi_1 = \varphi_1(r, t, \xi, \eta) = \frac{1}{\chi_1 r} \delta(r - \xi) \delta(t - \eta) \quad (7a)$$

for $0 \leq \xi \leq R_1$,

$$\varphi_2 = \varphi_3 = 0 \quad \text{respectively for } R_1 \leq \xi \leq R_2 \quad (7b)$$

or $R_2 \leq \xi \leq R_3$.

On the right side (7a) is the product of the displaced Dirac delta functions. The Green's function should fulfill conditions similar to (4)–(6)

$$G_i = 0 \quad \text{for } t < \eta, \quad i = 1, 2, 3, \quad (8)$$

$$\left. \frac{\partial G_3}{\partial r} \right|_{r=R_3} = -\frac{\alpha}{\lambda_3} [G_3] \Big|_{r=R_3}, \quad (9)$$

$$G_i \Big|_{r=R_i} = G_{i+1} \Big|_{r=R_i}, \quad i = 1, 2, \quad t \geq \eta, \quad (10a)$$

$$\lambda_i \left. \frac{\partial G_i}{\partial r} \right|_{r=R_i} = \lambda_{i+1} \left. \frac{\partial G_{i+1}}{\partial r} \right|_{r=R_i}, \quad i = 1, 2, \quad t \geq \eta. \quad (10b)$$

After considering boundary (5), (9), continuity (6), (10), and initial (4), (8) conditions, using the appropriate Green's theorem [20] and Dirac delta function properties, temperature increase in the i -th region of the model can be represented by the following integral relation [20, 21]

$$v_i(r, t) = \frac{\chi_1}{\lambda_1} \int_0^t \int_0^{R_1} g_1(\xi, f) G_i(r, t, \xi, \eta) \xi \, d\xi \, d\eta, \quad (11)$$

$$\text{for } R_{i-1} \leq r \leq R_i, \quad t \geq \eta, \quad R_0 = 0, \quad i = 1, 2, 3,$$

where $g_1(\xi, f)$ is given by equation (3a) or (3b) (after conversion $r \rightarrow \xi$). The relatively simple form of the formula (11) results from the lack of heat sources in the second and third regions. The condition for using (11) is knowledge of the Green's function G_i . One of the ways to determine it is to solve a homogeneous (or simpler) auxiliary problem using two methods: separation of variables [16, 20] and Green's function (7)–(10). By appropriate comparison of such solutions, one can determine the Green's function. The aforementioned homogenous auxiliary problem in relation to the function $\Psi_i(r, t)$ is defined as below

$$\frac{\partial^2 \Psi_i(r, t)}{\partial r^2} + \frac{1}{r} \frac{\partial \Psi_i(r, t)}{\partial r} - \frac{1}{\chi_i} \frac{\partial \Psi_i(r, t)}{\partial t} = 0 \quad (12)$$

$$\text{for } R_{i-1} \leq r \leq R_i, \quad R_0 = 0, \quad t > 0, \quad i = 1, 2, 3,$$

$$\left. \frac{\partial \Psi_3(r, t)}{\partial r} \right|_{r=R_3} = -\frac{\alpha}{\lambda_3} \Psi_3(r = R_3, t) \quad \text{for } t > 0, \quad (13)$$

$$\Psi_i(R_i, t) = \Psi_{i+1}(R_i, t) \quad \text{for } i = 1, 2 \quad \text{and } t > 0, \quad (14a)$$

$$\lambda_i \left. \frac{\partial \Psi_i(r, t)}{\partial r} \right|_{r=R_i} = \lambda_{i+1} \left. \frac{\partial \Psi_{i+1}(r, t)}{\partial r} \right|_{r=R_i} \quad (14b)$$

$$\text{for } i = 1, 2 \quad \text{and } t > 0,$$

$$\begin{aligned} \Psi_1(r, 0) &= F_1(r) \quad \text{for } 0 \leq r \leq R_1 \quad \text{and} \\ \Psi_i(r, 0) &= 0 \quad \text{for } R_{i-1} \leq r \leq R_i \quad \text{and } i = 2, 3, \end{aligned} \quad (15)$$

where $F_1(r)$ is any distribution of the initial condition in the first region.

Firstly, the boundary-initial problem (12)–(15) was solved by the separation of variables [16, 20]. According to the method, after separating time and location variables and rejecting the singular component for the $r = 0$ the following was obtained

$$\begin{aligned} \Psi_1(r, t) &= \sum_{n=1}^{\infty} C_n J_0(\gamma_n r / R_1) \cdot e^{-\gamma_n^2 \frac{\chi_1}{R_1^2} t} \\ &\text{for } 0 \leq r \leq R_1, \quad t > 0, \end{aligned} \quad (16)$$

$$\begin{aligned} \Psi_2(r, t) &= \sum_{n=1}^{\infty} (D_n J_0(\gamma_n s_1 r / R_1) + E_n Y_0(\gamma_n s_1 r / R_1)) \\ &\cdot e^{-\gamma_n^2 \frac{\chi_1}{R_1^2} t} \quad \text{for } R_1 \leq r \leq R_2, \quad t > 0, \end{aligned} \quad (17)$$

$$\begin{aligned} \Psi_3(r, t) &= \sum_{n=1}^{\infty} (F_n J_0(\gamma_n s_1 s_2 r / R_1) + H_n Y_0(\gamma_n s_1 s_2 r / R_1)) \\ &\cdot e^{-\gamma_n^2 \frac{\chi_1}{R_1^2} t} \quad \text{for } R_2 \leq r \leq R_3, \quad t > 0. \end{aligned} \quad (18)$$

where: $s_1 = \sqrt{\chi_1 / \chi_2}$, $s_2 = \sqrt{\chi_2 / \chi_3}$, γ_n are dimensionless eigenvalues of the boundary-initial problem (12)–(15), C_n, D_n, E_n, F_n, H_n are the coefficients of eigenfunctions and $J_k(\dots), Y_k(\dots)$ are the Bessel functions of the first and second kinds of order k .

Then the eigenvalues of the problem (12)–(15) were determined. In order to achieve that, continuity (14a), (14b) and boundary (13) conditions were used. After substituting the distributions (16)–(18) to (14a), (14b) and (13), a homogeneous system of five equations was obtained with respect to the unknown coefficients C_n, D_n, E_n, F_n, H_n

$$C_n J_0(\gamma_n) - D_n J_0(\gamma_n s_1) - E_n Y_0(\gamma_n s_1) = 0, \quad (19)$$

$$\begin{aligned} D_n J_0(\gamma_n p_1 s_1) + E_n Y_0(\gamma_n p_1 s_1) - \\ - F_n J_0(\gamma_n p_1 s_1 s_2) - H_n Y_0(\gamma_n p_1 s_1 s_2) = 0, \end{aligned} \quad (20)$$

$$K_1 C_n J_1(\gamma_n) - D_n J_1(\gamma_n s_1) - E_n Y_1(\gamma_n s_1) = 0, \quad (21)$$

$$\begin{aligned} K_2 D_n J_1(\gamma_n p_1 s_1) + K_2 E_n Y_1(\gamma_n p_1 s_1) - \\ - F_n J_1(\gamma_n p_1 s_1 s_2) - H_n Y_1(\gamma_n p_1 s_1 s_2) = 0, \end{aligned} \quad (22)$$

$$\begin{aligned} F_n (\varepsilon \cdot J_0(p_1 p_2 s_1 s_2 \gamma_n) / (\gamma_n s_1 s_2) - J_1(p_1 p_2 s_1 s_2 \gamma_n)) + \\ + H_n (\varepsilon \cdot Y_0(p_1 p_2 s_1 s_2 \gamma_n) / (\gamma_n s_1 s_2) - \\ - Y_1(p_1 p_2 s_1 s_2 \gamma_n)) = 0, \end{aligned} \quad (23)$$

where:

$$\begin{aligned} K_1 &= \lambda_1 / (\lambda_2 s_1), \quad K_2 = \lambda_2 / (\lambda_3 s_2), \quad \varepsilon = \alpha R_1 / \lambda_3, \\ p_1 &= R_2 / R_1, \quad p_2 = R_3 / R_2. \end{aligned}$$

The system of equations given above has a non-trivial solution if its main determinant is zeroed

$$\begin{aligned} \Delta(\gamma_n) &= a_1 [b_1 b_2 + b_3 b_4 + b_5 b_6 + b_7 b_8] - \\ &- a_2 [b_9 b_2 + b_{10} b_4 + b_{11} b_6 + b_{12} b_8] = 0, \end{aligned} \quad (24)$$

where:

$$\begin{aligned}
 a_1 &= \varepsilon \cdot Y_0(p_1 p_2 s_1 s_2 \gamma_n) / (\gamma_n s_1 s_2) - Y_1(p_1 p_2 s_1 s_2 \gamma_n), \\
 a_2 &= \varepsilon \cdot J_0(p_1 p_2 s_1 s_2 \gamma_n) / (\gamma_n s_1 s_2) - J_1(p_1 p_2 s_1 s_2 \gamma_n), \\
 b_1 &= K_1 J_1(\gamma_n) J_1(\gamma_n p_1 s_1 s_2), \\
 b_2 &= J_0(\gamma_n s_1) Y_0(\gamma_n p_1 s_1) - Y_0(\gamma_n s_1) J_0(\gamma_n p_1 s_1), \\
 b_3 &= K_2 J_0(\gamma_n) J_0(\gamma_n p_1 s_1 s_2), \\
 b_4 &= J_1(\gamma_n s_1) Y_1(\gamma_n p_1 s_1) - Y_1(\gamma_n s_1) J_1(\gamma_n p_1 s_1), \\
 b_5 &= K_1 K_2 J_1(\gamma_n) J_0(\gamma_n p_1 s_1 s_2), \\
 b_6 &= Y_0(\gamma_n s_1) J_1(\gamma_n p_1 s_1) - J_0(\gamma_n s_1) Y_1(\gamma_n p_1 s_1), \\
 b_7 &= J_0(\gamma_n) J_1(\gamma_n p_1 s_1 s_2), \\
 b_8 &= Y_1(\gamma_n s_1) J_0(\gamma_n p_1 s_1) - J_1(\gamma_n s_1) Y_0(\gamma_n p_1 s_1), \\
 b_9 &= K_1 J_1(\gamma_n) Y_1(\gamma_n p_1 s_1 s_2), \\
 b_{10} &= K_2 J_0(\gamma_n) Y_0(\gamma_n p_1 s_1 s_2), \\
 b_{11} &= K_1 K_2 J_1(\gamma_n) Y_0(\gamma_n p_1 s_1 s_2), \\
 b_{12} &= J_0(\gamma_n) Y_1(\gamma_n p_1 s_1 s_2).
 \end{aligned}$$

Relationship (24) is the equation of eigenvalues.

Additionally, using the system of equations (19)–(23) given above, the number of unknown coefficients can be reduced. For this purpose, the first four equations (19)–(22) were used. As a result, coefficients D_n, E_n, F_n, H_n were made dependent on one C_n . The coefficients determined in this way were substituted to (17), (18) and, after appropriate reduction, the following was obtained

$$\Psi_2(r, t) = \sum_{n=1}^{\infty} C_n Z_0(\gamma_n s_1 r / R_1) \cdot e^{-\gamma_n^2 \frac{\chi_1}{R_1^2} t} \quad (25)$$

for $R_1 \leq r \leq R_2, \quad t > 0,$

$$\Psi_3(r, t) = \sum_{n=1}^{\infty} C_n \Lambda_0(\gamma_n s_1 s_2 r / R_1) \cdot e^{-\gamma_n^2 \frac{\chi_1}{R_1^2} t} \quad (26)$$

for $R_2 \leq r \leq R_3, \quad t > 0,$

where

$$\begin{aligned}
 Z_k(\gamma_n s_1 r / R_1) &= w_1 J_k(\gamma_n s_1 r / R_1) + w_2 Y_k(\gamma_n s_1 r / R_1), \\
 \Lambda_k(\gamma_n s_1 s_2 r / R_1) &= w_3 J_k(\gamma_n s_1 s_2 r / R_1) + w_4 Y_k(\gamma_n s_1 s_2 r / R_1),
 \end{aligned}$$

$$\begin{aligned}
 w_1 &= \frac{K_1 J_1(\gamma_n) Y_0(\gamma_n s_1) - J_0(\gamma_n) Y_1(\gamma_n s_1)}{J_1(\gamma_n s_1) Y_0(\gamma_n s_1) - J_0(\gamma_n s_1) Y_1(\gamma_n s_1)}, \\
 w_2 &= \frac{J_0(\gamma_n) J_1(\gamma_n s_1) - K_1 J_1(\gamma_n) J_0(\gamma_n s_1)}{J_1(\gamma_n s_1) Y_0(\gamma_n s_1) - J_0(\gamma_n s_1) Y_1(\gamma_n s_1)}, \\
 w_3 &= (b_6 b_{11} + b_2 b_9 + b_4 b_{10} + b_8 b_{12}) / b_{13},
 \end{aligned}$$

$$w_4 = -(b_5 b_6 + b_1 b_2 + b_3 b_4 + b_7 b_8) / b_{13},$$

$$\begin{aligned}
 b_{13} &= (J_1(\gamma_n s_1) Y_0(\gamma_n s_1) - J_0(\gamma_n s_1) Y_1(\gamma_n s_1)) \cdot \\
 &\cdot (J_1(\gamma_n p_1 s_1 s_2) Y_0(\gamma_n p_1 s_1 s_2) - \\
 &- J_0(\gamma_n p_1 s_1 s_2) Y_1(\gamma_n p_1 s_1 s_2)).
 \end{aligned}$$

The form of equation (16) remained unchanged.

The unknown coefficient C_n in (16), (25), (26) has yet to be determined. For this purpose, initial conditions (15) were used. After substituting distributions (16), (25), (26) to (15) the following was obtained

$$\sum_{n=1}^{\infty} C_n J_0(\gamma_n r / R_1) = F_1(r) \quad \text{for } 0 \leq r \leq R_1, \quad (27)$$

$$\sum_{n=1}^{\infty} C_n Z_0(\gamma_n s_1 r / R_1) = 0 \quad \text{for } R_1 \leq r \leq R_2, \quad (28)$$

$$\sum_{n=1}^{\infty} C_n \Lambda_0(\gamma_n s_1 s_2 r / R_1) = 0 \quad \text{for } R_2 \leq r \leq R_3. \quad (29)$$

Subsequently, the relation (27) was multiplied by $(\lambda_1 / \chi_1) \cdot J_0(\gamma_m r / R_1)$ and integrated in the range $\langle 0, R_1 \rangle$. Analogous operations were performed on expressions (28), (29) (respectively multiplied by $(\lambda_2 / \chi_2) \cdot Z_0(\gamma_m s_1 r / R_1), (\lambda_3 / \chi_3) \cdot \Lambda_0(\gamma_m s_1 s_2 r / R_1)$ and integrated in ranges $\langle R_1, R_2 \rangle, \langle R_2, R_3 \rangle$). The relations obtained in this way were added to each other. Subsequently, the orthogonality condition of eigenfunctions of the radial coordinate in cylindrical multi-region systems (proven in [20, 22]) was used

$$\begin{aligned}
 &\frac{\lambda_1}{\chi_1} \int_0^{R_1} r J_0(\gamma_n r / R_1) J_0(\gamma_m r / R_1) dr + \\
 &+ \frac{\lambda_2}{\chi_2} \int_{R_1}^{R_2} r Z_0(\gamma_n s_1 r / R_1) Z_0(\gamma_m s_1 r / R_1) dr + \\
 &+ \frac{\lambda_3}{\chi_3} \int_{R_2}^{R_3} r \Lambda_0(\gamma_n s_1 s_2 r / R_1) \Lambda_0(\gamma_m s_1 s_2 r / R_1) dr = \\
 &= \begin{cases} 0 & \text{for } \gamma_n \neq \gamma_m \\ \|N(m)\|^2 & \text{for } \gamma_n = \gamma_m \end{cases} \quad (30)
 \end{aligned}$$

where $\|N(m)\|^2$ – square of the norm (32).

After calculating the suitable integrals in (30), ordering and replacing $m \rightarrow n$, the C_n coefficient was obtained

$$C_n = \frac{(\lambda_1 / \chi_1) \cdot \int_0^{R_1} r F_1(r) J_0(\gamma_n r / R_1) dr}{\|N(n)\|^2} \quad (31)$$

where

$$\begin{aligned} \|N(n)\|^2 = & \frac{\lambda_1}{2\chi_1} R_1^2 (J_0^2(\gamma_n) + J_1^2(\gamma_n)) + \\ & + \frac{\lambda_2}{2\chi_2} R_2^2 (Z_0^2(p_1 s_1 \gamma_n) + Z_1^2(p_1 s_1 \gamma_n)) - \\ & - \frac{\lambda_2}{2\chi_2} R_1^2 (Z_0^2(s_1 \gamma_n) + Z_1^2(s_1 \gamma_n)) + \\ & + \frac{\lambda_3}{2\chi_3} R_3^2 (\Lambda_0^2(p_1 p_2 s_1 s_2 \gamma_n) + \Lambda_1^2(p_1 p_2 s_1 s_2 \gamma_n)) - \\ & - \frac{\lambda_3}{2\chi_3} R_2^2 (\Lambda_0^2(p_1 s_1 s_2 \gamma_n) + \Lambda_1^2(p_1 s_1 s_2 \gamma_n)). \end{aligned} \quad (32)$$

Then the integration variable was changed in (31) ($r \rightarrow \xi$). The expression thus modified was substituted to (16), (25), (26). The relations obtained in this way were compared to the general solution of the problem (12)–(15) by Green's function method [20]. This leads to the sought Green's functions (after conversion $t \rightarrow t - \eta$)

$$G_1(r, t, \xi, \eta) = \frac{\lambda_1}{\chi_1} \sum_{n=1}^{\infty} \frac{J_0(\gamma_n \xi / R_1) J_0(\gamma_n r / R_1)}{\|N(n)\|^2} \cdot e^{-\gamma_n^2 \frac{\chi_1}{R_1^2} (t - \eta)}, \quad (33)$$

$$G_2(r, t, \xi, \eta) = \frac{\lambda_1}{\chi_1} \sum_{n=1}^{\infty} \frac{J_0(\gamma_n \xi / R_1) Z_0(\gamma_n s_1 r / R_1)}{\|N(n)\|^2} \cdot e^{-\gamma_n^2 \frac{\chi_1}{R_1^2} (t - \eta)}, \quad (34)$$

$$G_3(r, t, \xi, \eta) = \frac{\lambda_1}{\chi_1} \sum_{n=1}^{\infty} \frac{J_0(\gamma_n \xi / R_1) \Lambda_0(\gamma_n s_1 s_2 r / R_1)}{\|N(n)\|^2} \cdot e^{-\gamma_n^2 \frac{\chi_1}{R_1^2} (t - \eta)} \quad (35)$$

where $\|N(n)\|^2$ is given by the formula (32).

4. Time-and space-variable heating curves, time constants and steady-state current ratings

The time-and space-variable heating curves were determined separately for direct current (DC) and for alternating current (AC). After substituting (33)–(35) to (11), using (3b), (1) and introducing the DC index, time-and space-variable-step responses of the system were obtained (for $f = 0$)

$$T_{1DC}(r, t) = T_a + \sum_{n=1}^{\infty} M_n J_0(\gamma_n r / R_1) \varphi_n(t) \quad (36)$$

for $0 \leq r \leq R_1, \quad t > 0,$

$$T_{2DC}(r, t) = T_a + \sum_{n=1}^{\infty} M_n Z_0(\gamma_n s_1 r / R_1) \varphi_n(t) \quad (37)$$

for $R_1 \leq r \leq R_2, \quad t > 0,$

$$T_{3DC}(r, t) = T_a + \sum_{n=1}^{\infty} M_n \Lambda_0(\gamma_n s_1 s_2 r / R_1) \varphi_n(t) \quad (38)$$

for $R_2 \leq r \leq R_3, \quad t > 0,$

where

$$M_n = g_{DC} R_1^4 J_1(\gamma_n) / (\chi_1 \gamma_n^3 \|N(n)\|^2), \quad (39a)$$

$$\varphi_n(t) = \left(1 - e^{-\gamma_n^2 \frac{\chi_1}{R_1^2} t} \right). \quad (39b)$$

After using (3a) and making analogous substitutions, time-and space-variable heating curves were obtained in the case of alternating current

$$T_1(r, t) = T_a + \sum_{n=1}^{\infty} P_n L_n J_0(\gamma_n r / R_1) \varphi_n(t) \quad (40)$$

for $0 \leq r \leq R_1, \quad t > 0,$

$$T_2(r, t) = T_a + \sum_{n=1}^{\infty} P_n L_n Z_0(\gamma_n s_1 r / R_1) \varphi_n(t) \quad (41)$$

for $R_1 \leq r \leq R_2, \quad t > 0,$

$$T_3(r, t) = T_a + \sum_{n=1}^{\infty} P_n L_n \Lambda_0(\gamma_n s_1 s_2 r / R_1) \varphi_n(t) \quad (42)$$

for $R_2 \leq r \leq R_3, \quad t > 0,$

where

$$P_n = R_1^2 / (\chi_1 \gamma_n^2 \|N(n)\|^2), \quad (42a)$$

$$L_n = \int_0^{R_1} g_1(\xi, f) J_0(\gamma_n \xi / R_1) \xi \, d\xi \quad (42b)$$

and $g_1(\xi, f)$ is given by equation (3a) (after conversion $r \rightarrow \xi$). The integral (42b) is calculated numerically. In turn, stationary distributions (among others, necessary to determine the steady-state current rating) are calculated from (36)–(42) for $t \rightarrow \infty$. It boils down to zeroing the exponential function found in (39b).

One of the most important parameters describing the dynamics of the thermal field is the thermal time constant $\tau_i(r)$. It allows one to approximate the heating curve at a given point in the field using the step response of a first-order lag

$$T_i(r, t) = T_i(r, t \rightarrow \infty) [1 - \exp(-t/\tau_i(r))] + T_i(r, t = 0) \exp(-t/\tau_i(r)). \quad (43a)$$

The following relationship follows from the above formula [23, 27]

$$\tau_i(r) = \int_0^{\infty} \frac{T_i(r, t) - T_i(r, t \rightarrow \infty)}{T_i(r, t = 0) - T_i(r, t \rightarrow \infty)} dt \quad (43b)$$

for $i = 1, 2, 3.$

The parameter discussed also allows one to estimate the duration of the transient state as $4\tau_i(r)$ and determine the rate of temperature rise at any point in the field. After substitution (36)–(38) to (43b) was obtained in the case of direct current (DC)

$$\tau_{1DC}(r) = \frac{R_1^2 \sum_{n=1}^{\infty} A_n(r)/\gamma_n^2}{\chi_1 \sum_{n=1}^{\infty} A_n(r)}, \quad (44)$$

where $A_n(r) = J_0(\gamma_n r/R_1) S_n$ for $0 \leq r \leq R_1$,

$$\tau_{2DC}(r) = \frac{R_1^2 \sum_{n=1}^{\infty} B_n(r)/\gamma_n^2}{\chi_1 \sum_{n=1}^{\infty} B_n(r)}, \quad (45)$$

where $B_n(r) = Z_0(\gamma_n s_1 r/R_1) S_n$ for $R_1 \leq r \leq R_2$,

$$\tau_{3DC}(r) = \frac{R_1^2 \sum_{n=1}^{\infty} U_n(r)/\gamma_n^2}{\chi_1 \sum_{n=1}^{\infty} U_n(r)}, \quad (46)$$

where

$$U_n(r) = \Lambda_0(\gamma_n s_1 s_2 r/R_1) S_n \quad \text{for } R_2 \leq r \leq R_3, \quad (46a)$$

and

$$S_n = J_1(\gamma_n) / \left(\gamma_n^3 \|N(n)\|^2 \right). \quad (46b)$$

Local time constants in the case of alternating current are similar to those given above. The only difference compared to (44)–(46) is the integral relationship (42b), which appears in the functions $A_n(r)$, $B_n(r)$, $U_n(r)$.

In the Mathematica [24] environment, a programme was developed to calculate time- and space-variable heating curves and other system parameters. As an example, the busbar described in Section 2 was analysed. The following data were assumed:

$$\begin{aligned} R_1 &= 0.011 \text{ m}; & c_1 &= 400 \text{ J/(kg K)}; & \delta_1 &= 8700 \text{ kg/m}^3; \\ R_2 &= 0.01235 \text{ m}; & c_2 &= 1110 \text{ J/(kg K)}; & \delta_2 &= 1800 \text{ kg/m}^3; \\ R_3 &= 0.01535 \text{ m}; & c_3 &= 2800 \text{ J/(kg K)}; & \delta_3 &= 950 \text{ kg/m}^3; \\ \lambda_1 &= 360 \text{ W/(mK)}; & \lambda_2 &= 0.17 \text{ W/(mK)}; \\ \lambda_3 &= 0.27 \text{ W/(mK)}; & \alpha &= 14.31 \text{ W/(m}^2\text{K)}; \\ \rho(52.5^\circ\text{C}) &= 1.92481 \cdot 10^{-8} \text{ } \Omega\text{m}; & T_a &= 25^\circ\text{C}. \end{aligned} \quad (47)$$

The total heat transfer coefficient α occurring in (47) was determined based on an iterative method (IEC standard) [1]. Distributions (36)–(42) are fast-convergent series. Consequently, the summation in (36)–(42) was limited to twenty-five terms.

One of the most critical parameters of the busbars is the steady-state current rating I_{cr} . It is limited by the maximum value T_{\max} of the temperature to which the adhesive layer can heat up under sustained operating working conditions (the softening point is $85^\circ\text{C} \pm 5^\circ\text{C}$). In the case under consideration a smaller value was assumed $T_{\max} = 80^\circ\text{C}$. The adhesive layer is the most thermally exposed at the contact with copper (i.e., for $r = R_1$). Therefore, to determine the steady-state current rating, it is enough to solve the following equation with respect to I_{cr}

$$T_1(r = R_1, t \rightarrow \infty, I_{cr}) = T_{\max}. \quad (48)$$

Equation (48) was solved iteratively using the distribution (36) or (40) depending on the type of current (direct or alternating current). In the first case, the following was obtained: $I_{cr}(DC) = 1063.1 \text{ A}$. To conveniently observe the influence of frequency on the field distribution, the same root mean square value of the current was assumed in all cases $I = I_{cr}(DC)$. Using relations (36)–(42), heating curves were calculated at selected points of the system for $f = 0, 50, 100 \text{ Hz}$. The results are shown in Fig. 2. Fig. 3 shows the change in the stationary temperature (i.e., (36)–(42) at $t \rightarrow \infty$) over a wider frequency range at selected points of the busbar (at the same current load as before). On the other hand, Fig. 4 shows the dependence of the local time constant on the radial coordinate for the same cases of direct and alternating current. As one can see, the corresponding curves overlap (are the same).

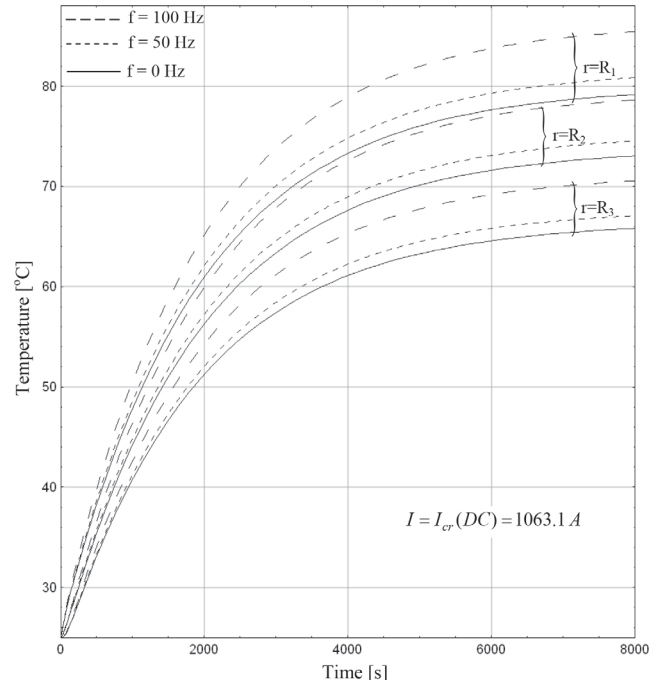


Fig. 2. Heating curves at selected points of the busbar in the case of direct current ($f = 0 \text{ Hz}$) and alternating current ($f = 50 \text{ Hz}$, $f = 100 \text{ Hz}$) with the same rms current $I = I_{cr}(DC) = 1063.1 \text{ A}$ in all cases.

It is also interesting change the steady-state current rating as a function of its frequency (assuming a constant maximum

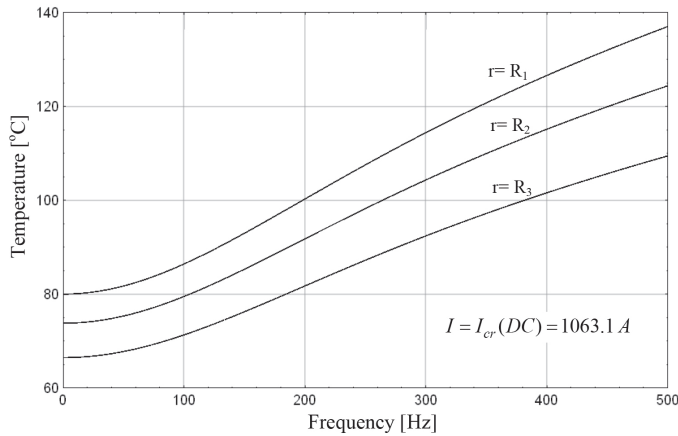


Fig. 3. Change of the stationary temperature ($t \rightarrow \infty$) at selected points of the busbar as a function of frequency with the same current load of the system $I = I_{cr}(DC) = 1063.1 A$.

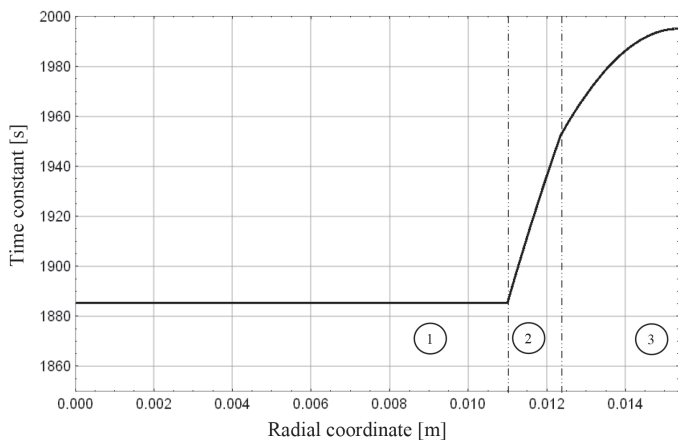


Fig. 4. Local time constant of the busbar as a radial coordinate function in the case of direct and alternating current ($f = 0, 50, 100 \text{ Hz}$, $I = I_{cr}(DC) = 1063.1 A$).

temperature of the adhesive layer $T_{max} = 80^\circ\text{C}$). Therefore, on the basis of (40) and (48), the graph shown in Fig. 5 was plotted.

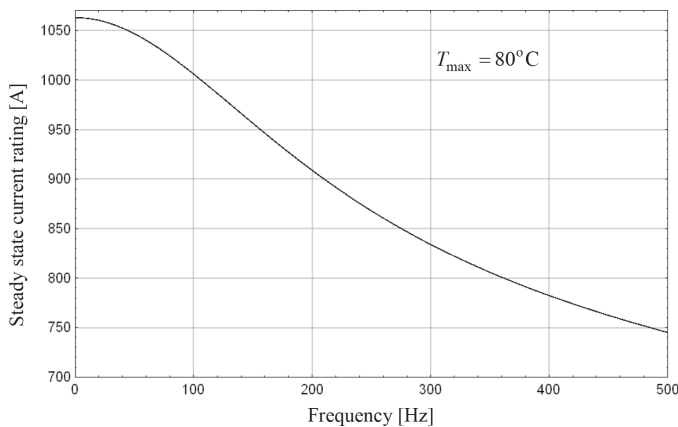


Fig. 5. Steady-state current rating of the busbar as a function of frequency assuming a constant maximum temperature of the adhesive layer $T_{max} = 80^\circ\text{C}$.

In addition, the basic relationships (36)–(42) were verified. For this purpose, the increments (1) were substituted to (2), (4)–(6). The resulting boundary-initial problem was solved again using the finite element method (FEM) [25]. It forms the basis of the professional NISA v.16 software [26], which was used for numerical analysis. Subsequently, the relative differences of temperature increases were calculated according to the following formula

$$\delta T_i = 100\% \frac{[T_i(r,t) - T_a] - [T_{iFE}(r,t) - T_a]}{T_i(r,t) - T_a}, \quad (49)$$

for $i = 1, 2, 3,$

where $T_i(r,t)$ is the temperature distribution obtained with the Green's method in the i -th region, $T_{iFE}(r,t)$ means the temperature distribution calculated by the finite element method in the i -th region, T_a is ambient temperature.

In Green's method, the truncation errors of the infinite series (36)–(42) can be arbitrarily reduced changing the value of threshold level in the summation procedure. Also errors are limited by the precision floating-point arithmetic of computers. In turn, the finite element method (FEM) errors are several orders of magnitude greater than the accuracy level of floating-point arithmetic. Therefore, Green's method is more accurate, the results of which are benchmark values (denominator of formula (49)).

Fig. 6 shows the relation (49) at selected points of the busbar. For better clarity, the graph was limited to the case $f = 0$ Hz and $f = 100$ Hz.

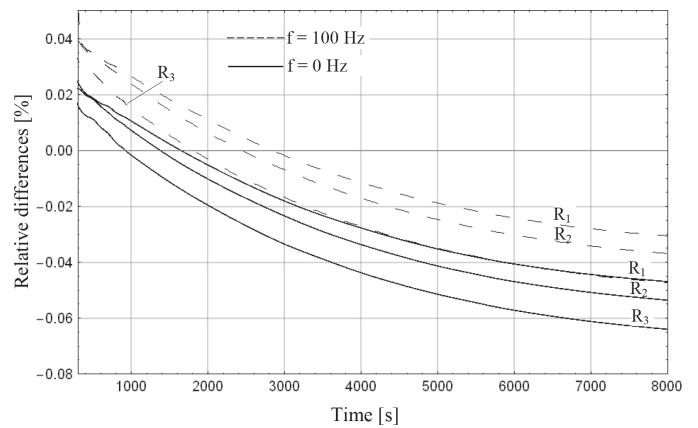


Fig. 6. Relative differences in heating curves increments determined by means of the finite element and Green's methods in the case of direct current ($f = 0 \text{ Hz}$) and alternating current ($f = 100 \text{ Hz}$).

5. Final remarks

A. The presented heating curves (Fig. 2) and stationary thermal profiles (Fig. 3) show that the frequency has a significant impact on the thermal field of the busbar. As one can see in Fig. 2 and Fig. 3, at the same current value, the increase in frequency results in temperature rising at any point

of the busbar. For example, in a steady state (Fig. 3), the temperature difference between the AC and DC models at $f = 100$ Hz is equal to $T_1(R_1, t \rightarrow \infty, f = 100 \text{ Hz}) - T_1(R_1, t \rightarrow \infty, f = 0 \text{ Hz}) = 6.4^\circ\text{C}$ and at $f = 500$ Hz it reaches the value of $T_1(R_1, t \rightarrow \infty, f = 500 \text{ Hz}) - T_1(R_1, t \rightarrow \infty, f = 0 \text{ Hz}) = 56.9^\circ\text{C}$. The physical reason for this is the increase in the electrical resistance of the conductor as a result of the increase in frequency [4]. Consequently, the amount of heat released in copper increases.

- B. Fig. 5 shows that, assuming a constant maximum temperature of the adhesive layer T_{\max} , the increase in frequency causes an apparent decrease in the steady-state current rating. This is also due to the increase in electrical resistance along with the frequency [4].
- C. Due to the increase of the electrical resistance, the frequency affects the volume density of the generated power (i.e. the right side of (2)). According to the laws of the dynamics of physical systems, forcing function does not change the time constant. In other words, the constant characterizes the system and is not related to the frequency of the input signal. Moreover, in the adopted model, the thermal (i.e. $\lambda_i, c_i, \delta_i, \alpha$) and geometric (R_1, R_2, R_3) parameters are constant. From this it follows that the distribution of the local time constant does not depend on frequency. Fig. 4 confirms the above-mentioned. One can see the correlation between Figs. 2 and 4. For the smallest value of the local time constant (i.e., for $0 \leq r \leq R_1$, Fig. 4) the heating curves increase the fastest (Fig. 2). In turn, for the largest time constant (i.e., for $R_2 \leq r \leq R_3$, Fig. 4) the temperature changes the slowest (Fig. 2).
- D. In the analysed time range (Fig. 6), the relative differences (49) of heating curves increments calculated using the Green's method and finite element method are small (within the range $(-0.08\%, 0.05\%)$). It should be noted that equation (49) was determined in the most unfavourable locations $r = R_i$ for $i = 1, 2, 3$. It results from the smallest accuracy of the finite element method on the border of different materials. However, Fig. 6 proves an excellent coincidence of analytical and numerical solutions.

Acknowledgements. The paper was prepared in Technical University of Białystok within the framework of project S/WE/2/18 sponsored by the Ministry of Science and Higher Education.

REFERENCES

- [1] G.J. Anders, *Rating of electric power cables: ampacity computations for transmission, distribution, and industrial applications*, McGraw-Hill Professional, New York, 1997.
- [2] R.T. Coneybeer, W.Z. Black, and R.A. Bush, "Steady-state and transient ampacity of bus bar", *IEEE Transactions on Power Delivery* 9 (4), 1822–1829 (1994).
- [3] M.K. Kazimierzczuk, *High-frequency magnetic components*, Wiley Publishing, 2009.
- [4] V.T. Morgan, "The current distribution, resistance and internal inductance of linear power system conductors – a review of explicit equations", *IEEE Transactions on Power Delivery* 3 (28), 1252–1262 (2013).
- [5] J. Acero, C. Carretero, I. Lope, R. Alonso, and J.M. Burdio, "Analytical solution of the induced currents in multilayer cylindrical conductors under external electromagnetic sources", *Applied Mathematical Modelling* 40, 10667–10678 (2016).
- [6] U.R. Patel, B. Gustavsen, and P. Triverio, "An equivalent surface current approach for the computation of the series impedance of power cables with inclusion of skin and proximity effect", *IEEE Transactions on Power Delivery* 4 (28), 2474–2482 (2013).
- [7] U.R. Patel and P. Triverio, "A complete model for computing the impedance of cable systems including skin, proximity, and ground return effect", *IEEE Transactions on Power Delivery* 5 (30), 2110–2118 (2015).
- [8] W. Mingli and F. Yu, "Numerical calculations of internal impedance of solid and tubular cylindrical conductors under large parameters", *IEE Proceedings-Generation, Transmission and Distribution* 1 (151), 67–72 (2004).
- [9] K.E. Oughstun, "Asymptotic description of pulsed ultrawideband electromagnetic beam field propagation in dispersive, attenuative media", *Journal of the Optical Society of America A* 18 (7), 1704–1713 (2001).
- [10] N.A. Cartwright and K.E. Oughstun, "Uniform asymptotics applied to ultrawideband pulse propagation", *Society for Industrial and Applied Mathematics* 49 (4), 628–648 (2007).
- [11] L.D. Paarmann, *Design and Analysis of Analog Filters: A Signal Processing Perspective*, Springer Science & Business Media, 2006.
- [12] F. Yang, G. Enzner, and J. Yang, "Frequency-Domain Adaptive Kalman Filter With Fast Recovery of Abrupt Echo-Path Changes", *IEEE Signal Processing Letters* 24 (12), 1778–1782 (2017).
- [13] O. Chavez and F. Mendez, "Conjugate heat transfer in a bimetallic conductor with variable electric resistivity", *Applied Thermal Engineering* 31, 3420–3427 (2011).
- [14] O. Chavez, F. Godinez, F. Mendez, and A. Aguilar, "Prediction of temperature profiles and ampacity for monometallic conductor considering the skin effect and temperature-dependent resistivity", *Applied Thermal Engineering* 109, 401–412 (2016).
- [15] A. Jordan, A. Barka, and N. Benmouna, "Transient state temperature distribution in a cylindrical conductor with skin effect", *International Journal of Heat and Mass Transfer* 11 (30), 2446–2447 (1987).
- [16] M.J. Latif, *Heat conduction*, Springer-Verlag, Heidelberg, 2009.
- [17] Z.S. Kolenda and J.S. Szmyd, "Entropy generation minimization in transient heat conduction processes PART II – Transient heat conduction in solids", *Bull. Pol. Ac.: Tech.* 62 (4), 883–887 (2014).
- [18] K.D. Cole, A. Haji-Sheikh, J.V. Beck, and B. Litkouhi, *Heat conduction using Green's functions*, CRC Press, 2011.
- [19] K. Gnidzinska, G. de Mey, and A. Napieralski, "Heat dissipation and temperature distribution in long interconnect lines", *Bull. Pol. Ac.: Tech.* 58 (1), 119–124 (2010).
- [20] D.W. Hahn and M.N. Ozisik, *Heat Conduction*, John Wiley & Sons, New Jersey, 2012.
- [21] S. Kukla and U. Siedlecka, "Green's function for heat conduction problems in a multi-layered hollow cylinder", *Journal of Applied Mathematics and Computational Mechanics* 13 (3), 115–122 (2014).

Analysis of the influence of current frequency on the thermal field of the insulated busbar

- [22] S. Singh, P.H. Jain, and Rizwan-Uddin, “Analytical solution to transient heat conduction in polar coordinates with multiple layers in radial direction”, *International Journal of Thermal Sciences* 47, 261–279 (2008).
- [23] A. Brykalski, “Ein Beitrag zur Bestimmung der mittleren Zeitkonstante von Diffusionsprozessen”, *International Journal of Heat and Mass Transfer* 28 (3), 613–620 (1985).
- [24] Wolfram Research, Inc., *Mathematica*, Illinois: Wolfram Research Inc., 2018.
- [25] P. Nithiarasu, R.W. Lewis, and K.N. Seetharamu, *Fundamentals of the finite element method for heat and mass transfer*, John Wiley & Sons 2016.
- [26] Manuals for NISA v.16, *NISA Suite of FEA Software (CD-ROM)*, Cranes Software, Inc. Troy, MI, USA, 2008.
- [27] J. Gołębiowski and J. Forenc, “Parallel computations of the step response of a floor heater with the use of a graphics processing unit. Part 2: results and their evaluation”, *Bull. Pol. Ac.: Tech.* 61 (4), 949–954 (2013).